Materials Research, Vol. 12, 2009, 291-297

Texture analysis of deformation induced martensite in an AISI 301L stainless steel: microtexture and macrotexture aspects.

Hamilton Ferreira Gomes de Abreu[I, *]; Marcelo José Gomes da Silva[I]; Luís Flávio Gaspar Herculano[I]; H. Bhadeshia[II].

[I]*Universidade Federal do Ceará – UFC, Centro de Tecnologia, Departamento de Engenharia Metalúrgica e de Materiais, Campus do Pici Bloco, 714, Pici, 60455-760 Fortaleza - CE, Brazil*
[II]*University of Cambridge, Materials Science and Metallurgy, Pembroke Street, Cambridge CB2 3QZ, U.K*

Abstract
Experiments have been conducted to study the strain induced transformation from austenite to martensite in a metastable AISI 301LN austenitic stainless steel, deformed by uniaxial tension applied along rolling direction. Samples 10% and 20% deformed have shown the presence of α´ martensite phase. Measured pole figures of martensite phase were compared to calculated ones, assuming no variant selection and selection of variants where interaction between stress and the plate of martensite adds to the driving force of transformation for favoured variants. EBSD (electron back scatter diffraction) microtexture experiments and macrotexture X-ray diffraction were performed. The orientation distribution functions (ODFs) from measured pole figure data were calculated. The measured results were compared with calculated results in both polycrystalline and single crystal samples of austenite. The results showed that the textures calculated on the basis variant selection consistent with Patel and Cohen's theory, which emphasizes a mechanical component of free energy, were in good agreement with measurements.

Keywords- phase transformation, texture, martensite.

Introduction

Metastable stainless steels are promising engineering materials due to a rewarding combination of good corrosion resistance and mechanical properties. Their mechanical properties can be affected significantly by deformation induced martensitic transformation. Furthermore, in order to use these steels to their full potential, it is important that the mechanisms acting during the martensitic phase transformation are understood from a crystallographic point of view.

Deformation can induce the formation of martensite in austenitic stainless steels. The amount of martensite depends on processing parameters such as the stress state of the material, temperature and rate of deformation. The steel composition and stacking fault energy can also exert great influence (1-7). Certain stresses such as shear can induce martensitic transformation at temperatures near the martensite-start temperature (M_s). When external stresses are applied the work done contributes to the free energy change; either raising or lowering the M_s (8).

The interaction energy which provides the mechanical driving force for transformation is given by (8):

$$\Delta G_{MECH} = \sigma_N \zeta + \tau s \qquad (1)$$

where σ_N is the stress component normal to the habit plane, τ is the shear stress resolved on the habit plane in the direction of shear and ζ and s are the respective normal and shear strains associated with transformation (9).

The total free energy available for transformation is the sum of chemical and mechanical components; the latter one being zero in the absence of an applied stress (10):

$$\Delta G = \Delta G_{CHEM} + \Delta G_{MECH}$$

where ΔG_{CHEM} is the chemical free energy change accompanying transformation. It would be reasonable to assume that there is strong variant selection when the ratio of $\Delta G_{MECH}/\Delta G$ is large (10).

The transformation sequence $\gamma \rightarrow \varepsilon \rightarrow \alpha'$, where ε refers to hexagonal-close packed martensite, has been proposed for austenitic stainless steels deformed by tension and rolling by a variety of authors (11-14). On the other hand the direct transformation of austenite (γ) into the body-centred cubic form α' of martensite $\gamma \rightarrow \alpha'$ through dislocation reactions has been found to be possible by Nolze (15). Kundu and Bhadeshia have shown that it is not necessary to consider the two-stage sequential transformation of austenite first into ε and then into α' in order to calculated the transformation texture (16). In further work (17), they modelled the development of transformation texture in a deformed austenitic stainless steel using the crystallographic theory of martensite (18,19) and the interaction of austenite with applied stress following Patel's and Cohen's model (8).

In this work, the deformation induced martensite was characterized in samples of commercial austenitic stainless steel AISI 301 LN by a combination of XRD (X-ray diffraction) and EBSD (electron backscattered diffraction) techniques. Texture evolution in austenite and martensite was studied using pole figures measured in single grains of the distinct phases, and also by representing the crystallographic texture with orientation distribution functions (ODFs) of multi-grain areas of the steel. The ODF describes the frequency of occurrence of particular orientations in an Euler space (20). The measured textures have been compared against calculations based on the crystallographic theory of martensite.

Experimental

In this study, a commercial AISI 301 LN stainless steel bearing 17.91Cr, 6.53Ni, 1.80 Mn, 0.79Si, 0.17Mo, 0.18Cu, 0.10N (wt%) and balance of Fe was used. Samples were solution treated for one hour at 1100^{o}C. Specimens for tensile tests were fabricated in accordance with ASTM A370-3a standard, with 50 mm gauge length. The specimens were submitted to plastic deformations of 10%, 20% and up to rupture in a 25t-Instron machine. Figure 1 shows stress-strain curves for samples deformed 10%, 20% and deformed up to rupture. Samples for pole figure measurements by XRD and EBSD were extracted from tensile test samples from the gauge length region in accordance to figure 2.

A Philips X'Pert Pro X-ray diffractometer with Mo-K_α radiation tube with an attached monochromator was used for texture studies. Three incomplete pole figures for α'-martensite and for austenite with maximum tilt of 75° were measured. Orientation distribution functions (ODF) were calculated in Labotex software using ADC (arbitrary defined cells) method. Three pole figures for each phase were used in the ODF calculations. Sections of φ_2=constant were plotted. The texture of the product resulting from γ→α transformation was calculated with software *crystal_habit_poly.f* developed by Kundu (9) and available in the web address www.msm.cam.ac.uk/map.

The EBSD studies were performed on samples from the mid plane section of the deformed region of the tensile specimens. An Oxford Crystal 300 EBSD system attached to a Philips XL-30 SEM was used and the data analysed with the aid of HKL-Channel 5 software.

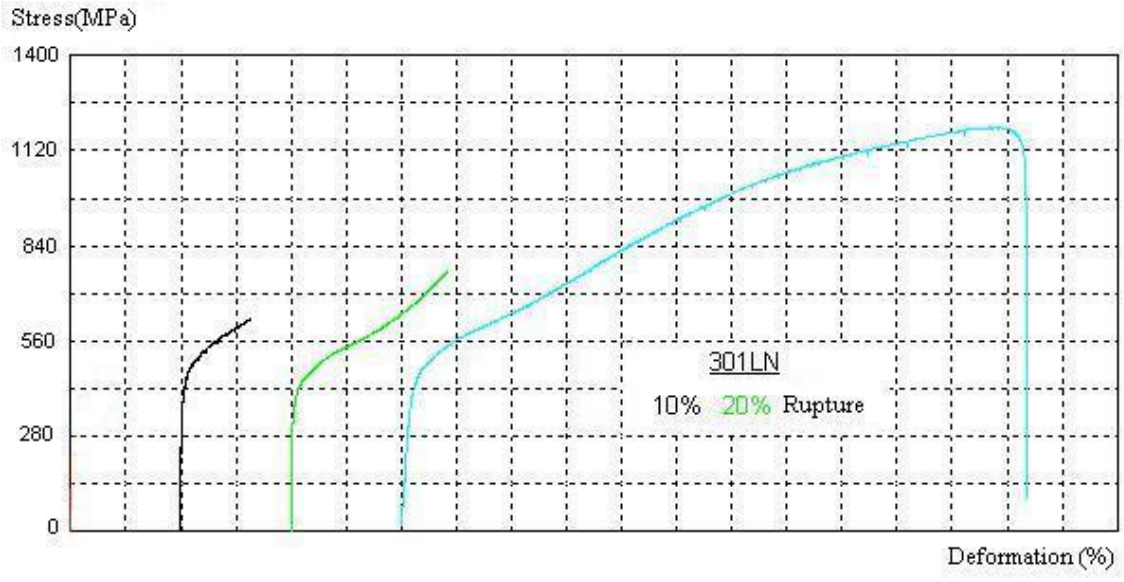

Figure 1 Stress-strain curves for samples deformed 10%, 20% and ruptured.

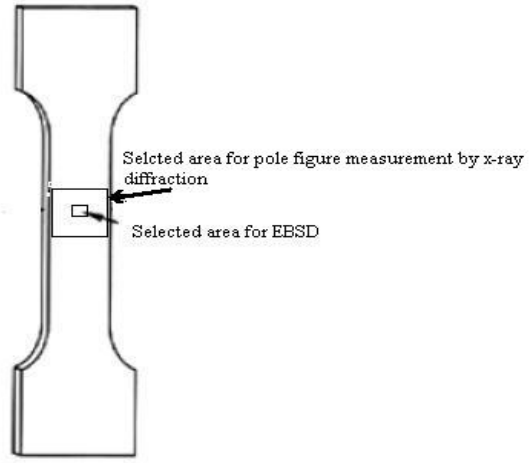

Figure 2- Sample for tensile test with indication of areas used for X-ray pole figures and EBSD analysis.

The same crystallographic set associated with a single martensite variant for an AISI 304 stainless steel reported by Kundu (17) was used in this study. The estimated lattice parameters for austenite and martensite are 0.3589 nm and 0.2873 nm respectively. This standard set is given as follows, calculated according to reference (21):

Habit plane (-0:183989 0:596344 - 0:781359)γ

Shape deformation matrix:

$$(\gamma P\gamma)= \begin{Bmatrix} 0.991342 & 0.028064 & -0.036770 \\ 0.028064 & 0.909040 & 0.119180 \\ 0.029429 & -0.095386 & 1.124979 \end{Bmatrix}$$

Coordinate transformation matrix :

$$(\gamma J\alpha)= \begin{Bmatrix} 0.579356 & 0.542586 & 0.102537 \\ 0.014470 & 0.133650 & -0.788984 \\ -0.552000 & 0.572979 & 0.086936 \end{Bmatrix}$$

Results

Figure 3 shows an EBSD orientation map for an undeformed sample. The observed microstructure is fully austenitic and some annealing twins are vividly revealed. The fact that no colour dominates is consistent with the absence of any strong texture.

Figure 4 shows orientation maps for a sample after 10% of deformation (a) austenite (b) martensite phases. After 10% of deformation, about 30% of austenite has transformed into α′ martensite. White regions in Figure 4a are α′ martensite. The orientation of martensite variants are in accordance with the color legend in figure 3b and can be seen in fig 4b. The stress was applied aligned with the vertical axis of the figure and martensite laths show an approximately 45° with the orientation of the applied stress. This is an indication of variant selection during martensitic transformation since the planes of maximum shear stress are located at 45° to the applied tensile stress.

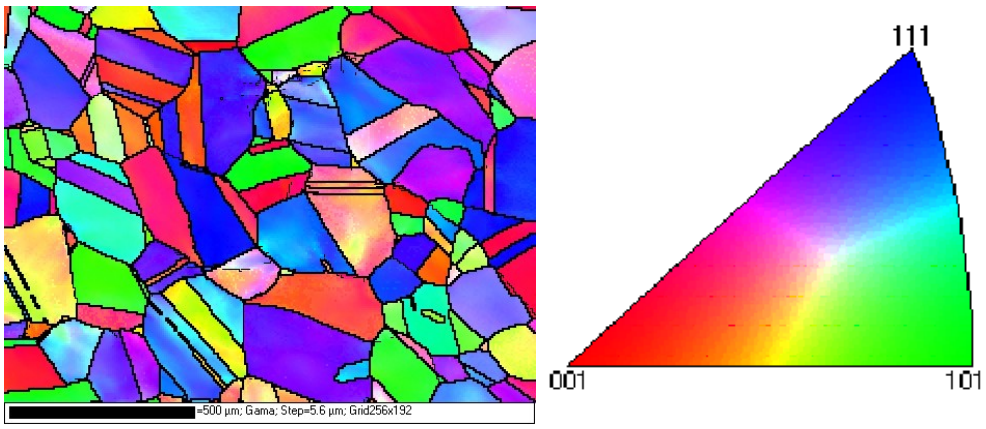

(a) (b)

Figure 3 – (a) EBSD orientation image for undeformed sample. (b) Colour key for crystallographic orientation. HAMILTON – THE MAGNIFICATION MARKERS

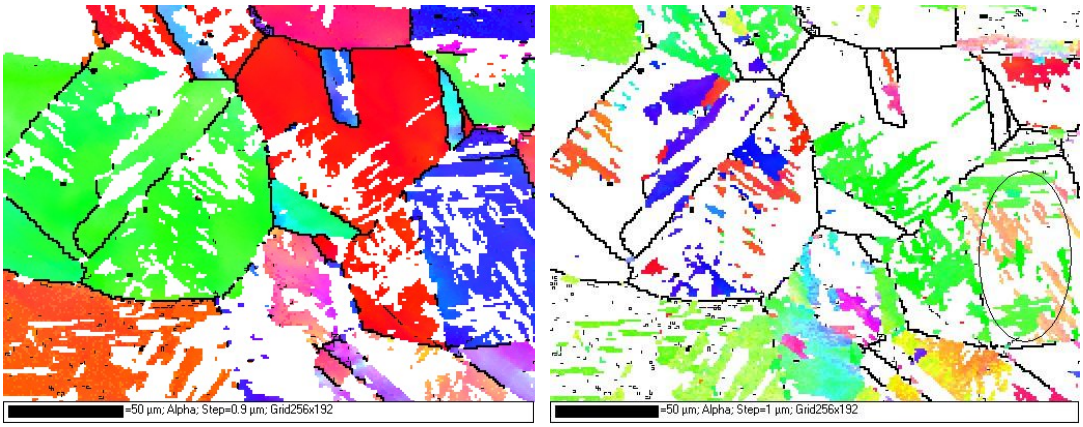

Figure 4 - EBSD orientation map for a sample with 10% of deformation (a) austenite (b) martensite. The orientation of the tensile stress is in the vertical direction.

Figure 5a shows the measured (100) α´ pole figure for the selected grain in Figure 4b (lower right corner). Figures 5b and 5c bring the calculated pole figures applying the crystallographic theory of martensite to the parent austenite grain, assuming that 24 and or the most favoured 12 variants form, respectively. When comparing the measured pole figure to the one calculated for 12 variants, it is clear that there is a variant selection process and the Patel and Cohen model (8) seems to be a good assumption.

The same procedure has been done for the 20% deformed sample (ε~0.18). The selected grain is the one on the right upper corner of Figure 6a. Figure 7 shows the (100) pole figures for the selected grain in Figure 6a; (a) measured; (b) calculated assuming no variant selection; (c) calculated assuming 12 of the most favoured variants. There is also a good match between measured pole figure and the calculated assuming Patel and Cohen model (8) with 12 variants acting. Some deviation between the calculated and measured intensities can be attributed to the fact that the large extent of plastic deformation may also deform the martensite into somewhat different orientations in space.

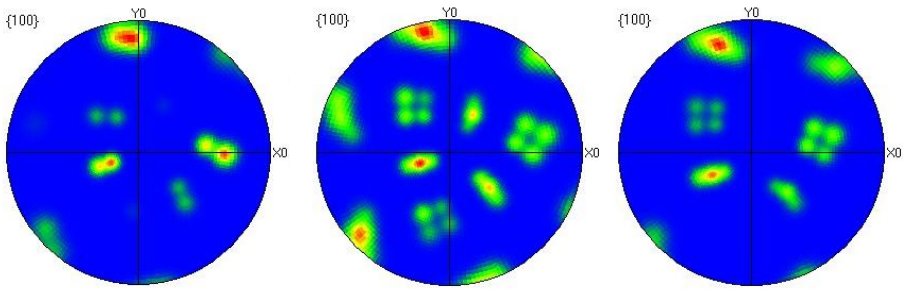

(a) (b) (c)

Figure 5- (100) Pole figures for the selected grain in fig. 4b; (a) measured; (b) calculated assuming no variant selection; (c) calculated assuming that 12 active variants.

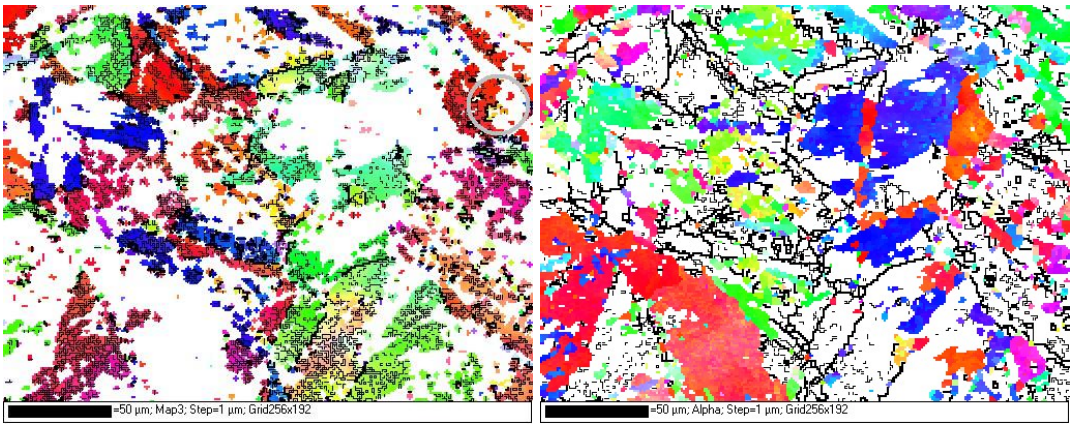

Figure 6- EBSD orientation map for a sample with 20% of deformation (a) austenite (b) martensite.

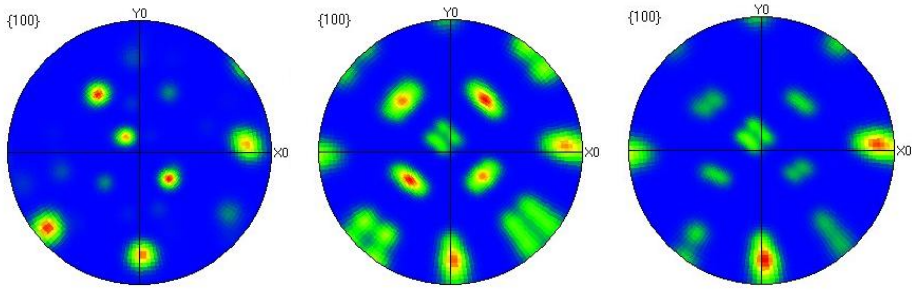

Figure 7- (100) Pole figures for the selected grain in fig. 5a; (a) measured; (b) calculated assuming no variant selection; (c) calculated assuming 12 most favoured variants.

The method (8,9) is now applied to analyze macrotexture. The austenite texture measured by X-ray diffraction as sown in Figure 8. The Copper ({112}<11-1>) component increases with deformation. The Goss component ({110}<001> decreases with deformation. With the Labotex software, 40,000 single grain orientations for each texture of austenite were generated. The set of 40,000 austenite orientation matrix was used as input to the transformation texture software *crystal_habit_poly.f* (9). The first condition assumed was that there was no variant selection so, for each austenite single orientation 24 martensite variants were generated. The second condition includes variant selection according to the mechanical free energy with only the 12 variants which comply with the applied stress permitted to form (8). It was assumed that all 12 of these variants grow in each austenite grain.

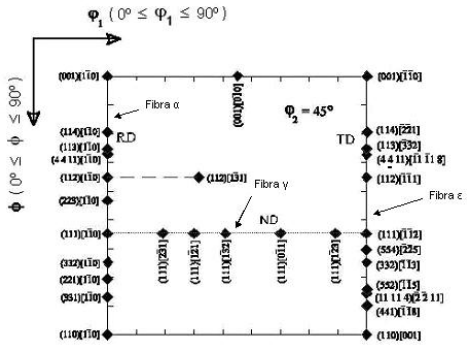

(a)

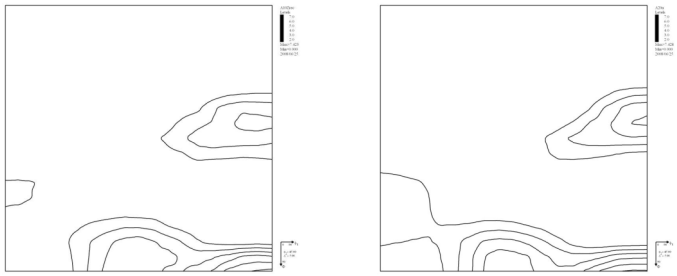

(b) (c)

Figure 8- φ2 = 45° ODF sections (a) ideal orientations in the section; (b) austenite deformed 10%; (c) austenite deformed 20%.

φ2 = 45° ODF sections for the induced martensite are presented in Figures 9 and 10 for the 10% and 20% deformed samples respectively. The first section (a) of each figure shows the measured ODFs. The second section (b) of each figure shows the calculated ODFs assuming no variant selection during the transformation process. Finally, the third (c) is based on the formation of the 12 favoured variants in each austenite grain. The shape of the measured ODFs is predicted with the assumption of the 12 favoured variants. The calculated ODFs assuming no variant selection present for both levels of deformation show sharp texture components {001}<110>. These components were not observed. It is clear that variant selection according to the mechanical free energy criterion is necessary to explain the observed macroscopic texture.

(a) (b) (c)

Figure 9- φ2 = 45° ODF sections for the induced martensite deformed 10% (a) measured ODF; (b) calculated ODF assuming that there is no variant selection; (c) calculated ODF assuming 12 of the most favoured variants.

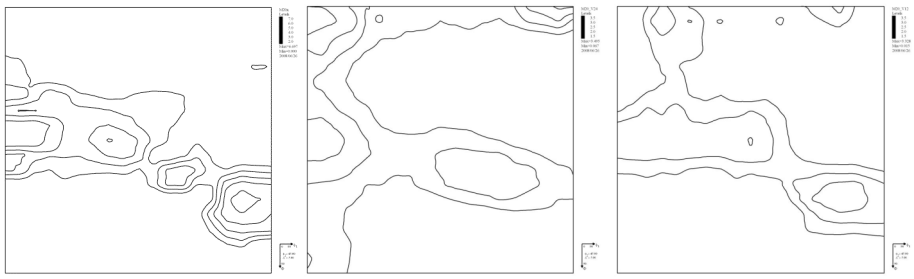

(a) (b) (c)

Figure 10- φ2 = 45° ODF sections for the induced martensite deformed 20% (a) measured ODF; (b) calculated ODF assuming that there is no variant selection; (c) calculated ODF assuming 12 of the most favoured variants.

Conclusion

Samples of austenitic stainless steel which have been deformed in tension to elongations ranging from 10-20% have been studied with respect to the development of transformation texture due to the formation of martensite.

In spite of the large plastic strains, it has been possible to estimate both the microtexture within individual austenite grains, and the macrotexture due to the transformation of a very large number of austenite grains. The method assumes that it is the stress which induces variant selection by favouring those crystallographic variants of martensite which when they form, act to relieve the applied stress. In other words, the Patel and Cohen selection criterion. Given this variant selection, the crystallographic theory of martensite has been used to predict the observed micro and macrotextures. In the latter case, deformation led to particular kinds of texture within the austenite, which were used as an input into the crystallographic model to estimate transformation macrotexture.

A neglect of variant selection results in a calculated texture which is inconsistent with observations.

Acknowledgements

We are grateful to the support from CNPq (National Council for Scientific and Technological Development), Project (200220/2007-1) and FUNCAP (Fundação Cearense de Apoio ao Desenvolvimento Científico e Tecnológico, project DCR 0053-07).

References

1. Padilha AF, Rios PR. Decomposition of Austenite in Austenitic Stainless Steels. ISIJ International. 2002;42(4):325-37.

2. Lecroisey F, Pineau A. Martensitic transformations induced by plastic deformation in the Fe-Ni-Cr-C system[J]. Metall Trans. 1972;3:387-96.

3. Olson GB, Cohen M. Kinetics of strain-induced martensitic nucleation. Metall Trans A. 1975;6A:791-5.

4. Olson GB, Cohen: M. Stress-assisted isothermal martensitic transformation: Application to TRIP steels. Metall Trans A. 1982;13A:1907-15.

5. Blanc G, Lacombe P, Baroux B, Beranger G. Stainless Steels - Les Editions de la Physique Les Ulis, Paris, France. 1993:595-611.

6. Nagy E, Mertinger V, Tranta F, Sólyom J. Study on bulk aluminum matrix nano-composite fabricated by ultrasonic dispersion of nano-sized SiC particles in molten aluminum alloy. 2004;378A:308-13.

7. Choi J-Y, Jin W. Strain induced martensite formation and its effect on strain hardening behavior in the cold drawn 304 austenitic stainless steels. Scripta Mater. 1997;36:99-104.

8. Patel JR, M.Cohen. Criterion for the action of applied stress in the martensitic transformation. Acta Materialia. 1953;1:531-8.

9. Kundu S. Transformation Strain and Crystallographic Texture in Steels. Cambridge: University of Cambridge; 2007.

10. Bhadeshia HKDH, David SA, Vitek JM, Reed RW. Stress-Induced Transformation to Bainite in a Fe-Cr-Mo-C Pressure Vessel Steel. Materials Science and Technology. 1991;7:686-98.

11. Mangonon PL, Thomas G. The martensite phases in 304 stainless steel. Metall Trans. 1970;1:1577-86.

12. Seetharaman V, Krishman P. INFLUENCE OF THE MARTENSITIC-TRANSFORMATION ON THE DEFORMATION- BEHAVIOR OF AN AISI-316 STAINLESS-STEEL AT LOW-TEMPERATURES. Journal of Materials Science. 1981;16:523.

13. Alteinberger I, Scholtes B, Martin V, Oetel H. Cyclic deformation and near surface microstructures of shot peened or deep rolled austenitic stainless steel AISI 304. Mat Sci Eng 1999;A264:1-16.

14. Petit B, Gey N, Cherkaoui M, Bolle B, Humpert M. Deformation behavior and microstructure/texture evolution of an annealed 304 AISI stainless steel sheet. Experimental and micromechanical modeling. Int J Plasticity. 2007;23:323-41.

15. Nolze G. Characterization of the FCC/BCC orientation relationship by ebsd using pole figures and variants. Metallkd. 2004;95(9):744-55.

16. Kundu S, Bhadeshia HKDH. Crystallographic texture and intervening transformations. Scripta Materialia. 2007;57:869 - 72.

17. Kundu S, Bhadeshia HKDH. Transformation texture in deformed stainless steel. Scripta Materialia. 2006;55:779 - 81.

18. Bowles JS, Mackenzie JK. The Crystallography of martensite transformations I. Acta Materialia. 1954;2:129-37.

19. Mackenzie JK, Bowles JS. The crystallography of martensite transformations II. Acta Materialia. 1954;2:138-47.

20. Randle V, Engler O. Introduction to texture analysis: macrotexture, microtexture and orientation mapping: Gordon and Beach Science Publishers; 2000.

21. Bhadeshia HKDH. Geometry of Crystals 2nd edition: Institute of Materials; 2001.